Materials Advances

PAPER

View Article Online
View Journal | View Issue

Cite this: *Mater. Adv.*, 2025, 6, 8960

UV-assisted rapid synthesis of high quality $CsPbBr_3$ perovskite single crystals

Mohammad A. Adeshina,†‡ Abdulazeez M. Ogunleye,‡ Hakseon Lee, Gunwoo Kim, Hyunmin Kim † and Jonghoo Park *

Received 6th June 2025,
Accepted 2nd October 2025

DOI: 10.1039/d5ma00595g

rsc.li/materials-advances

Inorganic halide perovskite single crystals have garnered significant interest due to their outstanding optical and electrical properties, making them strong candidates for a wide range of optoelectronic applications. However, conventional crystal growth techniques, such as the Bridgman, antisolvent, and inverse temperature crystallization (ITC) methods, often require complex procedures, high temperatures, and prolonged processing times. Here, we present a straightforward and efficient synthesis method for high-quality $CsPbBr_3$ perovskite single crystals based on ultraviolet (UV) light irradiation. This method employs UV light to provide the energy required for the $CsPbBr_3$ crystallization process, which includes molecularization, ionization, and nucleation. The single crystals synthesized using the UV method (UV-grown) exhibit an average carrier lifetime of 17 ns (twice that of ITC-grown counterparts) and a hole mobility of 197 $cm^2\ V^{-1}\ s^{-1}$ (a six-fold increase over ITC-grown counterparts). Our method not only provides enhanced optoelectronic properties but also simplifies the crystal synthesis process. This advancement paves the way for the scalable production of large-size $CsPbBr_3$ single crystals for in-depth fundamental studies and a wide range of optoelectronic applications.

Introduction

Inorganic halide perovskites, particularly $CsPbX_3$ (X = Cl, Br, and I), have gained attention for their superior stability, narrower emission bandwidth, and tunable photoluminescence (PL) wavelength in comparison to organic–inorganic hybrid perovskites.[1–4] These properties make them ideal for a variety of optoelectronic applications.[5–8] Although various synthesis methods for $CsPbX_3$, including the Bridgman, antisolvent, and inverse temperature crystallization (ITC) methods, have been successfully demonstrated for low defect $CsPbBr_3$ bulk single crystals, each approach has its own limitations.[9,10] The conventional Bridgman method is costly and requires sophisticated equipment and high temperatures, while the antisolvent method is time-consuming and demands precise stoichiometry. Although the ITC method significantly reduces the synthesis time, it still requires hours or days of regrowth stages to produce large-sized crystals.[11,12] Therefore, a strategy for the rapid synthesis of high-quality, scalable perovskite single crystals is still necessary.

Recently, interaction between light and the perovskite crystals has emerged as a promising method of enhancing the optoelectronic properties of perovskites. UV irradiation has been shown to induce significant changes in perovskite materials, including phase transformation,[13] photo-degradation,[14,15] and morphology modification[16] in both inorganic and hybrid colloidal 3D nanocrystals and 2D perovskite nano-plates. For instance, UV light exposure can trigger a structural phase transition in $CsPbBr_3$ nanocrystals, leading to changes in their optical and electronic properties.[17] These light-induced modifications demonstrate the profound impact of UV irradiation on perovskite materials at the nanoscale. Studies have revealed that $CsPbBr_3$ nanocrystals experience a reversible orthorhombic-to-cubic phase transition at moderate excitation light energy and become amorphous at higher light energy, demonstrating that light-driven phase transitions occur in perovskite materials.[18] Moreover, a photon-induced reversible phase transition from orthorhombic to tetragonal in $CsPbBr_3$ perovskite is reported, driven by Pb-Br octahedral torsion and the local coulombic field, enabling a fast and controllable response to light.[19] Light-induced lattice expansion plays a crucial role in enhancing the efficiency of perovskite solar cells as it was demonstrated that continuous light illumination induces a uniform lattice expansion in hybrid perovskite thin films, leading to improved device performance.[20,21] Additionally, surface layers of lead halide perovskite crystals exhibit high concentrations of positively charged vacancies and negatively charged halide ions, creating an electric field that increases the optical band gap near the surface after

School of Electronic and Electrical Engineering, Kyungpook National University, Daegu 41566, Republic of Korea. E-mail: jonghoopark@knu.ac.kr

† Present addresses: Division of Biotechnology, Daegu Gyeongbuk Institute of Science and Technology (DGIST), Daegu 42988, Republic of Korea.

‡ Equally contributing author.

photoexcitation.[22] Light excitation also enhances the ionic conductivity of methylammonium lead iodide, a key metal halide photovoltaic material, by several orders of magnitude, leading to a previously unexplored pathway for photodecomposition of the perovskite.[23] Furthermore, light has been shown to prompt the self-assembly of cubic $CsPbBr_3$ perovskite nanocrystals into nanowires, offering an efficient alternative for the synthesis of nanowires and other perovskite superstructures.[24] It has also been observed that exposing pre-synthesized nanocrystals to UV irradiation induces an increase in the size of the nanocrystals multiple fold.[25–27] However, the majority of studies have focused on nanocrystals, with relatively limited exploration into the use of UV irradiation for the growth of bulk single crystals.

In this study, we introduce a novel, straightforward, and rapid synthesis method for high-quality bulk $CsPbBr_3$ inorganic perovskite single crystals using UV light. To the best of our knowledge, this is the first report of utilizing UV light exposure to induce the molecularization, ionization, nucleation, and crystallization processes for the synthesis of bulk inorganic halide perovskite single crystals. The UV-assisted synthesis method leverages the UV light energy to drive the formative processes of the $CsPbBr_3$ perovskite precursor, leading to the growth of high-quality crystals. The resulting crystals exhibited a rectangular-shaped millimeter-sized morphology with an average length of 3 mm and a maximum of 5 mm achieved within 90 minutes. The optical and electronic characteristics of the UV-grown crystals were investigated using various techniques including X-ray diffraction, UV-vis absorption, photoluminescence, time-resolved lifetime decay measurements, Hall effect measurement, and Raman spectroscopy. Compared to the ITC-grown crystals, which had an average lifetime of 8.3 ns and a carrier mobility of 30 $cm^2\ V^{-1}\ s^{-1}$, the UV-grown perovskite crystals demonstrated higher photoluminescence efficiency, a carrier lifetime of 17 ns, and a significantly higher carrier mobility of 197 $cm^2\ V^{-1}\ s^{-1}$. Therefore, this study presents a compelling contribution to the field of inorganic halide perovskites, and is expected to inspire further research efforts in this direction.

Materials and methods

Cesium bromide (CsBr), lead(II) bromide ($PbBr_2$), methylammonium bromide (MABr), dimethylformamide (DMF) and dimethyl sulfoxide (DMSO) were purchased from Sigma-Aldrich and used without further purification.

$CsPbBr_3$ single crystal synthesis

Crystal synthesis was performed in two steps. The first step involved the preparation of the precursor solution, while the second step involved the UV irradiation of the precursor solution. In the first step, the CsBr and $PbBr_2$ compounds were weighed in a molar ratio of 1 to 2 and dissolved in DMSO solvent. The solution was stirred for 3 hours at room temperature to obtain a uniform and colorless solution. The solution was then filtered using a 0.2 μm Millipore filter to obtain a purified precursor solution. In the second step, 500 μL of the purified precursor solution was exposed to UV light for 1.5 hours to allow photoionization, nucleation, and crystal growth to occur. The irradiation was performed using a UVC-30s UV lamp (Jaesung Engineering CO.) with the following specifications: wavelength of 254 nm, power density of 25 mW cm^{-2}. The UV lamp was positioned directly above the uncovered precursor solution in a glass vial, ensuring uniform illumination across the sample surface. The resulting crystals were collected, cleaned with DMF, and dried.

ITC $CsPbBr_3$ single crystal synthesis

The ITC crystal growth was initiated by placing 500 μl of the precursor solution in a vial and heating it to 85 °C in an oil bath similar to earlier reports.[28,29] The vial was kept in the oil bath for 4 hours to generate crystal seeds. The crystal seeds were then regrown for 16 hours, cleaned with DMF, and dried.

$MAPbBr_3$ single crystal synthesis

A solution containing equimolar concentrations of MABr and $PbBr_2$ was prepared by dissolving them in DMF and stirring the mixture at room temperature for 3 hours. Following dissolution, the solution underwent filtration to obtain pure solutions. Subsequently, equal volumes of these solutions were subjected to both UV irradiation and the ITC growth method, mirroring the procedures previously employed for $CsPbBr_3$.

Characterization

Powder XRD measurement was carried out using Panalytical (EMPYREAN), with an X-ray generator: 4 kW, a vertical goniometer with scan range: $1.5 < 2\theta < 140$, and a sample stage (reflection-transmission spinner).

Steady-state absorption and photoluminescence spectra were measured using a UV-vis spectrometer (Perkin Elmer Lambda 950) and a fluorescence spectrometer (Horiba FluoroMax-4), respectively.

Photoluminescence quantum yield (PLQY) measurements were performed using an integrating sphere setup coupled to the fluorescence spectrometer. The absolute PLQY was calculated by comparing the integrated emission intensity to the integrated absorption intensity.

A time-resolved photoluminescence (TRPL) measurement study was carried out using a confocal microscope (MicroTime-200, Picoquant, Germany) with a 10× (air) objective. For the lifetime measurements, a single-mode pulsed diode laser (470 nm with a pulse width of ~30 ps and an average power of 30–100 nW operating in 1 MHz repetition rate) was used as an excitation source. A dichroic mirror (490 DCXR, AHF), a long-pass filter (HQ500lp, AHF), a 150 μm pinhole, a bandpass filter (500–600 nm, Thorlabs), and a single-photon avalanche diode (PDM series, MPD) were used to collect emission from the samples. A time-correlated single-photon counting system (PicoHarp-300, PicoQuant GmbH) was used to count emission photons. Exponential function fittings for the obtained PL decays were performed using Symphotime-64 software (Ver. 2.2).

The Hall mobility and carrier trap density measurements were carried out with the Ecopia HMS3000 system (magnetic

field of 0.51 T), using the Van der Pauw Hall effect measurement technique at room temperature.

Discussion

The synthesis of $CsPbBr_3$ single crystals using the UV irradiation technique is illustrated in Fig. 1. The UV light was directly illuminated onto the uncovered precursor in the preparatory bowl. When molecules absorb a UV light energy greater than its ionization energy, a photoionization process occurs, releasing electrons.[30,31] The ionization energies of the Cs^+ and $PbBr_3^-$ ions in the precursor are reported to be 3.85 eV and 4.31 eV, respectively, which fall within the range of our UV source energy (4.88 eV).[32,33] The DMSO serves as a coordinating solvent that modulates the precursor solubility, facilitates ion migration, and contributes to defect passivation. Its interaction with $PbBr_2$ helps stabilize intermediate complexes that are crucial for uniform nucleation under UV irradiation. Clusters consisting of Cs are particularly susceptible to ionization due to their low ionization energy compared to other elements.[34] The photoionization reaction process can be represented using the Born–Haber cycle. The Born–Haber cycle has traditionally been employed for analyzing formation enthalpies. In this case, it is utilized for analyzing the reaction enthalpy components of the UV-grown $CsPbBr_3$ crystal.[35–37] The formation process of $CsPbBr_3$ from solid CsBr and $PbBr_2$ compounds can be subdivided into several consecutive steps, as illustrated in eqn (1). The initial step is the molecularization of the CsBr denoted with ΔE_{mo}, which involves breaking the CsBr and $PbBr_2$ lattice structures and formation of Cs and $PbBr_3$ molecules. The next

$$\begin{aligned} &CsBr + PbBr_2 + DMSO \xrightarrow{\Delta E_{mo}} Cs + PbBr_3 \\ &Cs + PbBr_3 \xrightarrow{\Delta E_1} Cs^+ + PbBr_3 + e^- \\ &Cs^+ + PbBr_3 + e^- \xrightarrow{\Delta E_2} Cs^+ + PbBr_3^- \\ &Cs^+ + PbBr_3^- \xrightarrow{\Delta E_{latt}} CsPbBr_3 \end{aligned} \quad (1)$$

step is the ionization of the Cs molecule (ΔE_1 is Cs^+ ionization energy), followed by the ionization of $PbBr_3$ (ΔE_2 is $PbBr_3^-$ ionization energy). Finally, the amount of energy to form the inorganic perovskite structure is denoted as the lattice energy (ΔE_{latt}).

To further validate the effect of UV photoionization, two precursor solutions of a 0.1 molar solution of $CsPbBr_3$ precursor, which is 100 times dilution, were prepared. One solution was exposed to UV light (254 nm LED, 5 mW cm^{-2} power) treatment for 3 hours, while the other solution was not exposed to UV light. The optical properties of the $CsPbBr_3$ perovskite precursor solutions were investigated for the UV treated and non-treated samples. Fig. 2a shows the absorption spectrum of the untreated precursor solution, spanning from 240 to 310 nm (black line), while the absorption spectrum of the UV-treated $CsPbBr_3$ precursor solution shown in Fig. 2b exhibits a broader range from 240 nm to 350 nm (black line). Both the untreated and UV-treated solutions displayed an absorption peak around 285 nm, corresponding to the absorption spectrum of $PbBr_2$ while additional absorption peaks at approximately 310 nm and 322 nm in the UV-treated solution are attributed to the formation of $PbBr_3^-$ ions and a $Cs[PbBr_3]$ complex, respectively.[38–40] The exposure of the $CsPbBr_3$ precursor to UV facilitated the molecularization, ionization, nucleation and rapid lattice-growth rate of the $CsPbBr_3$ bulk single crystals. This method produces crystals with fewer defects, yielding higher intensity of the second-order phonon peak in the Raman spectrum of the UV-grown $CsPbBr_3$ single crystals as shown in Fig. S1 in the SI.[41,42] These findings provide valuable insights into the mechanism of UV-grown $CsPbBr_3$ single crystals. A thermocouple inserted into the precursor was used to measure its temperature during crystal growth under UV irradiation. As shown in Fig. S3, the precursor reached a maximum temperature of 55 °C during the entire growth process, which is lower than the temperature required for ITC, at least 85 °C.[11] This confirms that UV irradiation, rather than thermal effects, is the primary driver of crystallization. The structural characteristics of the $CsPbBr_3$ single crystals grown under different conditions were investigated using X-ray diffraction (XRD) analysis. Fig. 3a presents the XRD patterns of $CsPbBr_3$ crystals grown using the UV-assisted and ITC methods. The XRD patterns of the two growth conditions exhibited similar diffraction peaks, consistent with previously reported works on

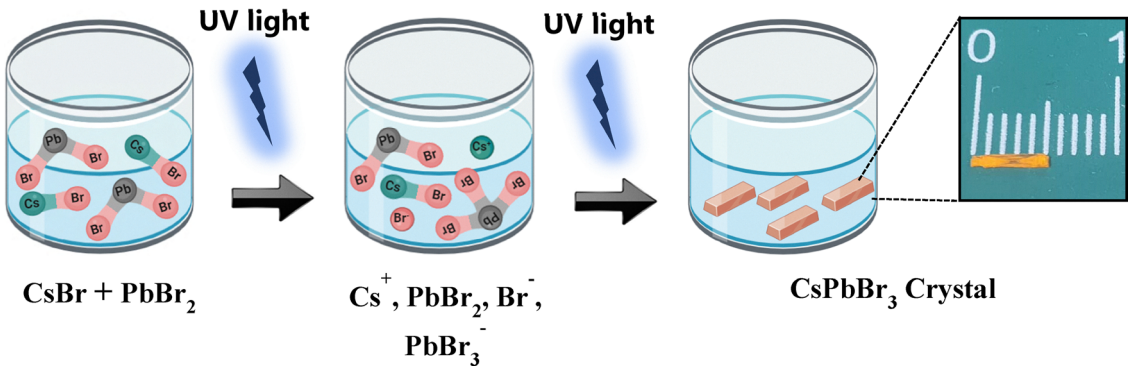

Fig. 1 Schematic illustration of chemical processes for the UV-assisted synthesis method of $CsPbBr_3$ crystals.

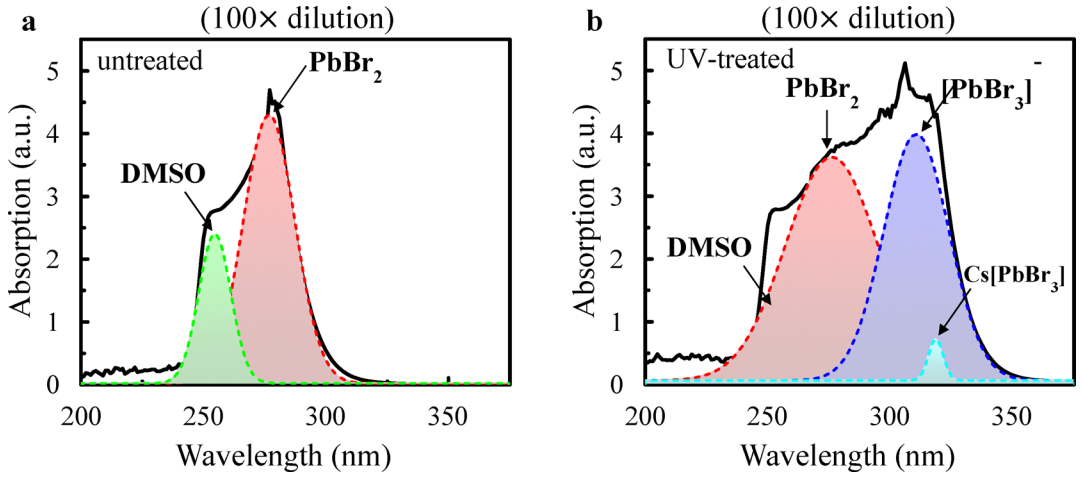

Fig. 2 Absorption spectra of the $CsPbBr_3$ precursor: (a) non-treated with a spectral range from 240 nm to 310 nm and (b) treated with UV with a spectral range from 240 nm to 350 nm.

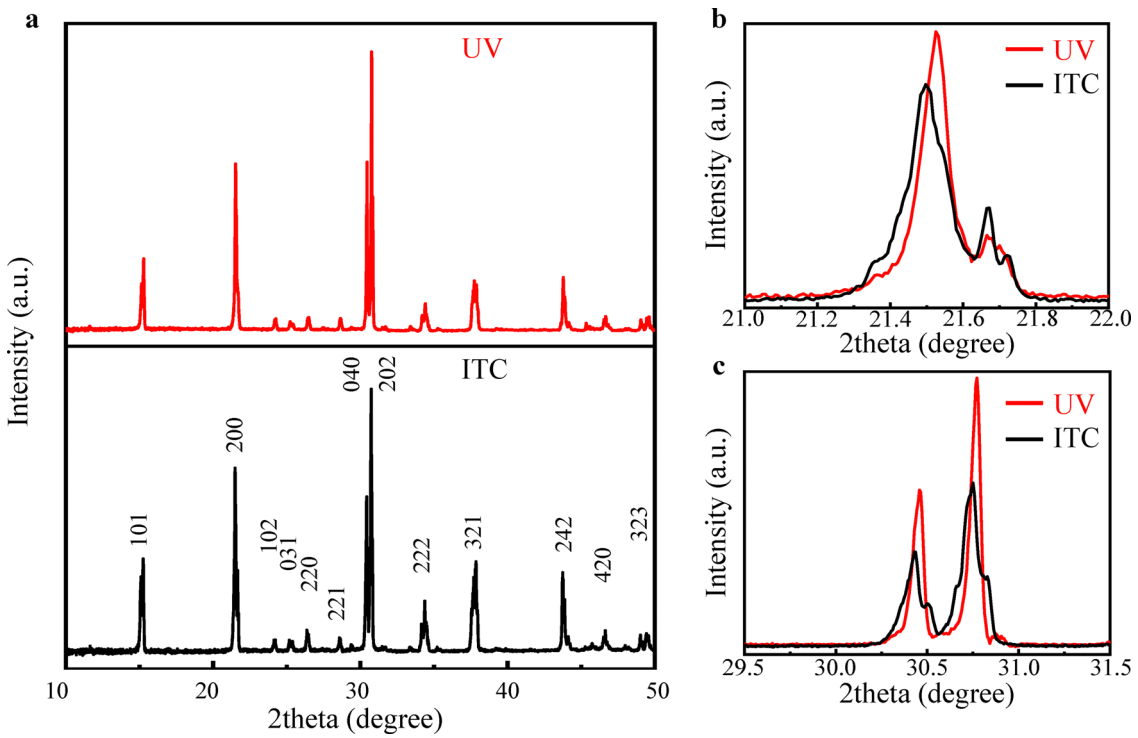

Fig. 3 (a) XRD plot for UV- and ITC-grown $CsPbBr_3$ and (b) enlarged XRD pattern of the peaks with higher intensity and narrower width at 21.0°–22.0° and (c) 29.5°–31.5°.

$CsPbBr_3$ single crystals.[28,29] The major diffraction peaks observed for the UV-grown crystals were located at 15.27°, 21.55°, 30.45°, 30.76°, 37.90°, and 43.78°, which can be indexed to the (101), (121), (040), (202), (123), and (242) planes of the orthorhombic $CsPbBr_3$ crystal structure (JCPDS No. 96-451-0746), respectively. Notably, the UV-grown crystals exhibited diffraction peaks with markedly higher intensity and significantly narrower width at the signature peaks, corroborating findings from previous studies.[43] Interestingly, the high-resolution XRD data revealed systematic shifts in the peak positions between the ITC-grown and UV-grown $CsPbBr_3$ samples. For instance, the (101) peak occurred at $2\theta \approx 15.253°$ for the ITC-grown sample, but shifted to $2\theta \approx 15.274°$ for the UV-grown samples (Fig. S4a). Similar trends were observed for other characteristic peaks, such as the (121) peak shifting from $2\theta \approx 21.497°$ in the ITC-grown sample to $2\theta \approx 21.528°$ in the UV-grown sample (Fig. S4b), and the (040) peak position changing from $2\theta \approx 30.432°$ for the ITC-grown sample to $2\theta \approx 30.458°$ for the UV-grown sample (Fig. S4c). These systematic peak shifts indicate that the UV-grown $CsPbBr_3$ crystals exhibit

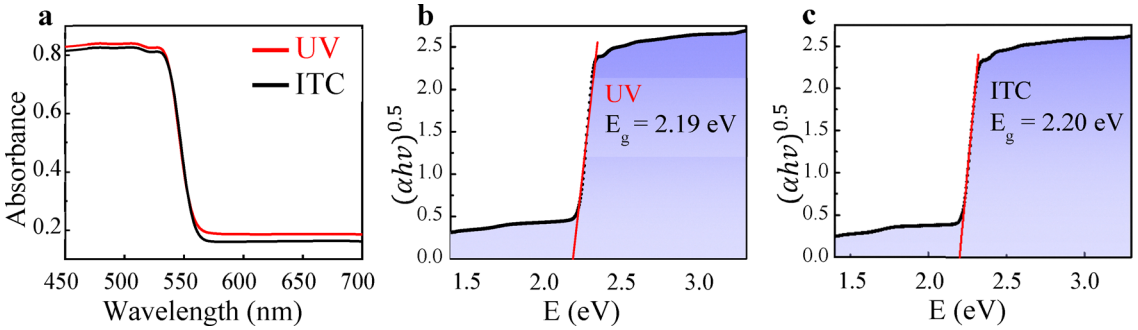

Fig. 4 (a) Absorbance curve of UV- and ITC-grown $CsPbBr_3$. Energy band gap from the Tauc plot of (b) UV-grown $CsPbBr_3$ and (c) ITC-grown $CsPbBr_3$.

a compressively strained lattice structure compared to the ITC-grown samples, resulting from differences in growth conditions and associated lattice distortions. These findings highlight the structural advantages of the UV-assisted synthesis method, which leads to improved material quality compared to the ITC-grown counterparts. Understanding the origins of these structural variations and their implications for the optoelectronic properties of the materials could provide valuable insights for optimizing the performance of $CsPbBr_3$ perovskite crystals.

The optical properties of the synthesized $CsPbBr_3$ crystals were investigated using UV-vis absorption spectroscopy. The synthesized crystals exhibited a sharp absorption edge at 565 nm, which indicates a highly crystalline structure (Fig. 4a). The optical band gap of the crystals was estimated using Tauc plots from the UV-vis absorbance spectra. The band gaps of the UV- and ITC-grown $CsPbBr_3$ crystals were 2.19 and 2.20 eV, respectively, as shown in Fig. 4b and c. These values are in good agreement with the theoretical values and are consistent with previously reported work.[44] The UV-grown crystal demonstrated a higher absorption compared to the ITC-grown crystal, which could be attributed to its improved crystal quality. These findings indicate that the UV photoionization method offers a favorable approach for synthesizing high-quality $CsPbBr_3$ crystals.

Fig. 5a shows the steady-state photoluminescence (PL) spectra of $CsPbBr_3$ crystals grown by both the UV and ITC methods. The PL spectra for both samples exhibited a peak at 528 nm, consistent with previously reported values.[45] The observed divergence between the absorption onset at 565 nm and the PL peak at 528 nm can be rationalized by considering the influence of defect-mediated absorption tails and exciton–phonon interaction. Such spectral offsets have been previously reported in $CsPbBr_3$ crystals, where the apparent red-shift in the absorption edge does not correspond to the bandgap.[46,47] Liu *et al.* demonstrated that the strong exciton–phonon coupling leads to absorption broadening, while PL remains centered at the band-edge emission energy.[48] Similarly, Falsini *et al.* attributed the extended absorption tails to the dynamic disorder and Urbach tail formation, whereas the PL emission reflected direct band-to-band transition.[49] In addition, Su *et al.* showed that $CsPbBr_3$ crystals grown by anti-solvent precipitation exhibit morphology-dependent optical responses, further indicating that the synthesis methods influence defect states and excitonic behavior.[50] Collectively, these findings support our assertion that the PL peak accurately represents band-edge recombination, while the absorption edge includes sub-bandgap contribution from the tail states. Furthermore, Fig. 5b shows the TRPL measurements that were conducted to calculate the carrier recombination lifetime of the $CsPbBr_3$ crystals by fitting the curve with an exponential time (τ_{ave})[51] function in eqn (2), where τ_i represents the carrier lifetime component and A_i represents the amplitude of the corresponding carrier lifetime. The average decay time (τ_{ave})

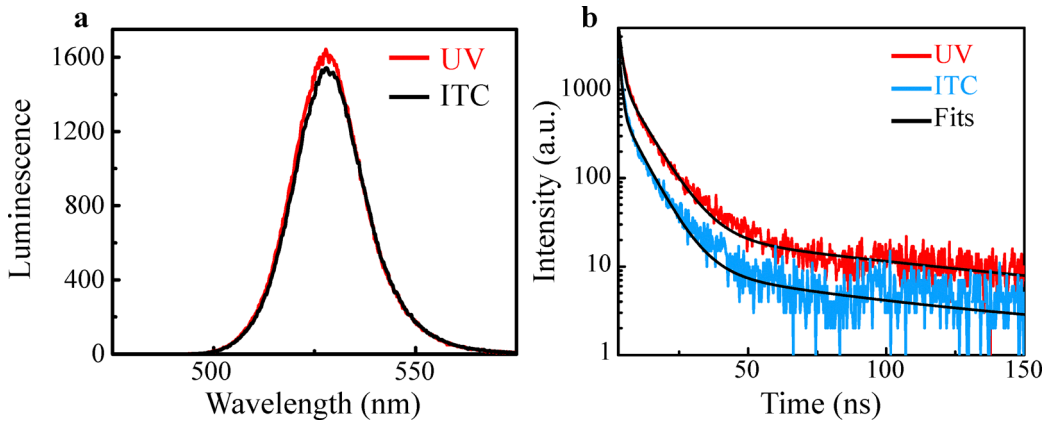

Fig. 5 (a) Photoluminescence spectra and (b) carrier lifetime decays of UV- and ITC-grown $CsPbBr_3$.

Table 1 Comparison of optoelectronic parameters and photoluminescent carrier lifetime of $CsPbBr_3$ crystals grown with various techniques

Crystal growth method	Life time (ns)	Trap density (cm^{-3})	Mobility ($cm^2\ V^{-1}\ s^{-1}$)	Charge type	Ref.
ITC[a]	233	1.1×10^{10}	52	Electron	44
Bridgeman	10.5	1.9×10^{9}	2300	Electron	56
Bridgeman	10.9	6.36×10^{9}	11.6	Electron	57
AVC[b]	6.8	2.8×10^{10}	13.6	—	58
AVC[b]	—	4.5×10^{7}	143	Hole	59
ITC[a]	6.2	7.1×10^{10}	28.5	Electron	28
LTC[c]	16.8	7.1×10^{10}	160	Electron	28
UV-photoionization	17	1.46×10^{9}	197	Hole	This work
ITC[a]	8.3	9.63×10^{9}	30	Hole	This work

[a] Inverse temperature crystallization method. [b] Antisolvent vapor-assisted method. [c] Low-temperature crystallization method.

reflects the recombination dynamics of carriers in the perovskite materials.

$$\langle \tau_{ave} \rangle = \frac{\sum_i A_i \tau_i^2}{\sum_i A_i \tau_i} \quad (2)$$

The parameters of the triexponential function fitted to time-resolved photoluminescence spectra are listed in Table S2 in the SI. In comparison to the average lifetime of 8.3 ns for the ITC-grown crystal, the UV-grown crystal exhibits a noticeably longer carrier lifetime decay of 17 ns at an excitation wavelength of 470 nm. The compact lattice structure, as evidenced by the angular shifts in the XRD data, reduces the density of defects and trap states, thereby suppressing non-radiative recombination and extending the carrier lifetime. This result shows that UV-grown crystals not only acquire higher crystallinity and lower defect density but also suppress nonradiative recombination near the crystal surface, which will result in enhanced optoelectronic performances.[52]

Finally, the electrical properties of the UV- and ITC-grown crystals are compared in Table 1, along with the results from previous studies. The dominant charge carriers were found to be holes in both crystals. The trap density was significantly lower in the UV-grown crystal compared to the ITC-grown crystal, indicating fewer defects that could hinder hole mobility and conductivity. Additionally, the hole mobility was significantly higher in the UV-grown (197 $cm^2\ V^{-1}\ s^{-1}$) crystal than the ITC-grown crystal (30 $cm^2\ V^{-1}\ s^{-1}$). This suggests that the UV-grown crystal provides a more favorable transport environment with reduced charge scattering caused by defects. The synergistic effect of reduced lattice strain, due to reduced interplanar spacing, and a more compact lattice structure in the UV-grown $CsPbBr_3$ crystals may be responsible for the simultaneous enhancement in carrier mobility and lifetime, key metrics for high-performance optoelectronic devices. The findings also highlight the importance of the growth method in determining the quality of semiconductor crystals and their suitability for various electronic applications. PLQY measurements conducted under uniform excitation conditions revealed that UV-grown $CsPbBr_3$ crystals exhibited a superior PLQY of 0.1%, markedly higher than the 0.07% observed in samples synthesized *via* ITC. The enhanced PL performance is indicative of suppressed non-radiative recombination pathways, attributed to reduced intrinsic defect densities and minimized deep level trap states, as substantiated by time-resolved photoluminescence spectroscopy. Extended carrier lifetime observed in the UV-grown samples further validates the efficacy of UV irradiation in mitigating defect formation during crystal nucleation and growth. These findings underscore the critical role of photonic treatment in engineering high-purity $CsPbBr_3$ crystals for advanced optoelectronic applications. The intrinsic properties of the UV-grown crystals, such as high crystallinity, sharp photoluminescence emission, and low trap density, are directly linked to their suitability for photodetector and light-emitting applications. These characteristics align well with the performance metrics reported by Gupta *et al.*,[10] where similar $CsPbBr_3$ crystals were successfully integrated into photodetector devices.

The UV-assisted synthesis method was applied for the growth of $MAPbBr_3$ single crystals. However, the photoluminescence and lifetime measurements, detailed in Fig. S5 of the SI, revealed a noticeable degradation in the lifetime performance of UV-grown crystals when compared to their counterparts grown through the ITC method. The diminished performance observed in the UV-grown crystals can be attributed to the degradation of the organic component within the methylammonium (MA) site induced by UV irradiation.[53–55]

Conclusion

In conclusion, this study demonstrated the novel growth method of high-quality $CsPbBr_3$ perovskite single crystals using UV irradiation. The UV-driven method facilitates the molecularization, ionization, nucleation, and lattice growth of $CsPbBr_3$ bulk single crystals, resulting in a high hole mobility of 197 $cm^2\ V^{-1}\ s^{-1}$ and extended carrier lifetime of 17 ns. These findings provide significant insights into the fundamental understanding of perovskite single crystals and represent an important step forward in advancing all-inorganic halide perovskite materials for optoelectronic applications. Further research on the development of thin films with this method could lead to the emergence of novel perovskite-based devices with improved performance and stability, thereby enabling the realization of next-generation optoelectronic technologies.

Author contributions

Conceptualization: J. P., M. A. A., A. M. O., methodology: J. P., M. A. A., A. M. O., supervision: J. P, funding acquisition: J.P. Experiment and measurement: M. A. A., A. M. O., H. L., G. K. Data analysis and investigation: J. P., M. A. A., A. M. O., and H. K. The manuscript was written through contributions of all authors. All authors have given approval to the final version of the manuscript.

Conflicts of interest

The authors declare no conflict of interest.

Data availability

The data supporting this article have been included as part of the supplementary information (SI). Supplementary information is available. See DOI: https://doi.org/10.1039/d5ma00595g.

Acknowledgements

This work was supported by a grant funded by the Korean government (MSIT) [NRF-2023R1A2C1007997]. The XRD, photoluminescence and lifetime measurements were performed at the Korea Basic Science Institute (KBSI), Daegu Center, Korea.

References

1 S. Ullah, *et al.*, All-inorganic $CsPbBr_3$ perovskite: a promising choice for photovoltaics, *Mater. Adv.*, 2021, **2**, 646–683.
2 Y. Pan, *et al.*, Progress in the preparation and application of $CsPbX_3$ perovskites, *Mater. Adv.*, 2022, **3**, 4053–4068.
3 J. Ahn, J. Park and S. J. Oh, All-Inorganic Metal Halide Perovskite (CsPbX3; X = Cl, Br, I) Nanocrystal-Based Photodetectors, *J. Sens. Sci. Technol.*, 2022, **31**, 383–388.
4 J. Xun, J. Deng, W. Shen, M. Li and R. He, Rapid synthesis of highly stable all-inorganic perovskite nanocrystals exhibiting strong blue luminescence, *J. Alloys Compd.*, 2021, **872**, 159612.
5 N. Marinova, *et al.*, Hindered Amine Light Stabilizers Increase the Stability of Methylammonium Lead Iodide Perovskite Against Light and Oxygen, *ChemSusChem*, 2017, **10**, 3760–3764.
6 J. Lu, *et al.*, Ultrafast Solar-Blind Ultraviolet Detection by Inorganic Perovskite $CsPbX_3$ Quantum Dots Radial Junction Architecture, *Adv. Mater.*, 2017, **29**, 1–8.
7 J. Lin, *et al.*, Direct Observation of Band Structure Modifications in Nanocrystals of $CsPbBr_3$ Perovskite, *Nano Lett.*, 2016, **16**, 7198–7202.
8 A. M. Ogunleye, M. A. Adeshina, G. W. Kim, H. Kim and J. Park, Bright Prospects, Lingering Challenges: $CsPbBr_3$ Quantum Dots for Environmental Sensing, *Cryst. Growth Des.*, 2025, **25**, 3252.
9 D. Wu, *et al.*, Advances in Perovskite Single Crystal Thin Films: Synthesis Methods and Applications in Photodetection, *Adv. Opt. Mater.*, 2024, 2401131.
10 R. Gupta, *et al.*, Synthesis and characterization of all-inorganic (CsPbBr 3) perovskite single crystals, *Mater. Adv.*, 2022, **3**, 7865–7871.
11 X. Wu, P. Li, X. Wei and J. Liu, All-Inorganic Perovskite Single Crystals for Optoelectronic Detection, *Crystals*, 2022, **12**, 1–35.
12 A. M. Ogunleye, *et al.*, Inherent Lattice Distortion Engineering via Magnetic Field for High-Quality Strained $MAPbI_3$ Perovskite Single Crystals, *Adv. Mater. Interfaces*, 2024, **12**, 2400781.
13 A. Sen, S. Chatterjee and P. Sen, UV-Assisted Conversion of 2D Ruddlesden-Popper Iodide Perovskite Nanoplates into Stable 3D MAPbI3Nanorods, *J. Phys. Chem. C*, 2022, **126**, 18057–18066.
14 A. Sen, S. Chatterjee and P. Sen, Proton-Mediated Structural and Optical Recovery of a UV-Degraded Colloidal Ruddlesden-Popper Perovskite Nanoplate for Prolonged Application, *ACS Appl. Nano Mater.*, 2023, **6**, 9130–9136.
15 S. K. Ha, C. M. Mauck and W. A. Tisdale, Toward Stable Deep-Blue Luminescent Colloidal Lead Halide Perovskite Nanoplatelets: Systematic Photostability Investigation, *Chem. Mater.*, 2019, **31**, 4.
16 Y. Wang, *et al.*, Photon Driven Transformation of Cesium Lead Halide Perovskites from Few-Monolayer Nanoplatelets to Bulk Phase, *Adv. Mater.*, 2016, **28**, 10637–10643.
17 J. Shamsi, *et al.*, Bright-Emitting Perovskite Films by Large-Scale Synthesis and Photoinduced Solid-State Transformation of $CsPbBr_3$ Nanoplatelets, *ACS Nano*, 2017, **11**, 10206–10213.
18 M. S. Kirschner, *et al.*, Photoinduced, reversible phase transitions in all-inorganic perovskite nanocrystals, *Nat. Commun.*, 2019, **10**, 504.
19 J. Xue, *et al.*, Photon-Induced Reversible Phase Transition in CsPbBr 3 Perovskite, *Adv. Funct. Mater.*, 2019, **29**, 1–8.
20 H. Tsai, *et al.*, Light-Induced Lattice Expansion Leads to High-Efficiency Perovskite Solar Cells, *Science*, 2018, **360**, 67.
21 N. Rolston, *et al.*, Comment on 'light-induced lattice expansion leads to high-efficiency perovskite solar cells', *Science*, 2020, **368**, 67–70.
22 S. P. Sarmah, *et al.*, Double Charged Surface Layers in Lead Halide Perovskite Crystals, *Nano Lett.*, 2017, **17**, 2021–2027.
23 G. Y. Kim, *et al.*, Large tunable photoeffect on ion conduction in halide perovskites and implications for photodecomposition, *Nat. Mater.*, 2018, **17**, 445–449.
24 J. Liu, *et al.*, Light-Induced Self-Assembly of Cubic $CsPbBr_3$ Perovskite Nanocrystals into Nanowires, *Chem. Mater.*, 2019, **31**, 6642–6649.
25 D. Esparza, S. Sidhik, T. López-Luke, J. M. Rivas and E. De La Rosa, Light-induced effects on crystal size and photostability of colloidal $CsPbBr_3$ perovskite nanocrystals, *Mater. Res. Express*, 2019, **6**, 45041.
26 V. Nagal, *et al.*, $CsPbBr_3$ Nanoplatelets: Synthesis and Understanding of Ultraviolet Light-Induced Structural

Phase Change and Luminescence Degradation, *ECS J. Solid State Sci. Technol.*, 2021, **10**, 096002.
27 J. Shamsi, *et al.*, Bright-Emitting Perovskite Films by Large-Scale Synthesis and Photoinduced Solid-State Transformation of $CsPbBr_3$ Nanoplatelets, *ACS Nano*, 2017, **11**, 10206–10213.
28 J. Peng, *et al.*, Crystallization of $CsPbBr_3$ single crystals in water for X-ray detection, *Nat. Commun.*, 2021, **12**, 1531.
29 P. Cheng, *et al.*, Growth and High-Performance Photodetectors of $CsPbBr_3$ Single Crystals, *ACS Omega*, 2023, **8**, 26351–26358.
30 E. G. Nazarov, R. A. Miller, G. A. Eiceman and J. A. Stone, Miniature differential mobility spectrometry using atmospheric pressure photoionization, *Anal. Chem.*, 2006, **78**, 4553–4563.
31 C. Chen, D. Jiang and H. Li, UV photoionization ion mobility spectrometry: Fundamentals and applications, *Anal. Chim. Acta*, 2019, **1077**, 1–13.
32 U. Hochkirch, W. Herrmann, R. Stößer, H.-H. Borchert and M. W. Linscheid, Electron Paramagnetic Resonance and Mass Spectrometry: Useful Tools to Detect Ultraviolet Light Induced Skin Lesions on a Molecular Basis-A Short Review, *J. Spectrosc.*, 2006, DOI: 10.1155/2006/196825.
33 C. Zheng and O. Rubel, Ionization Energy as a Stability Criterion for Halide Perovskites, *J. Phys. Chem. C*, 2017, **121**, 11977–11984.
34 H. G. Limberger and T. P. Martin, Photoionization spectra of cesium and cesium oxide clusters, *J. Chem. Phys.*, 1989, **90**, 2979–2991.
35 P. Cremaschi and M. Simonetta, Barmer to internal rotation in the methylammonium ion, *J. Mol. Struct.*, 1975, **29**, 39–45.
36 Y. R. Luo, *Comprehensive Handbook of Chemical Bond Energies*, CRC press, 2007, DOI: 10.1201/9781420007282.
37 S. J. Jeon, A. B. Raksit, G. I. Gellene and R. F. Porter, Formation of Hypervalent Ammoniated Radicals by Neutralized Ion Beam Techniques, *J. Am. Chem. Soc.*, 1985, **107**, 4129–4133.
38 A. Naikaew, *et al.*, Photoexcitation of perovskite precursor solution to induce high-valent iodoplumbate species for wide bandgap perovskite solar cells with enhanced photocurrent, *Sci. Rep.*, 2023, **13**, 1–12.
39 S. J. Yoon, K. G. Stamplecoskie and P. V. Kamat, How Lead Halide Complex Chemistry Dictates the Composition of Mixed Halide Perovskites, *J. Phys. Chem. Lett.*, 2016, **7**, 1368–1373.
40 Q. A. Akkerman, *et al.*, Controlling the nucleation and growth kinetics of lead halide perovskite quantum dots, *Science*, 2022, **377**, 1406–1412.
41 J. Ibaceta-Jaña, *et al.*, Vibrational dynamics in lead halide hybrid perovskites investigated by Raman spectroscopy, *Phys. Chem. Chem. Phys.*, 2020, **22**, 5604–5614.
42 Z. Zhao, *et al.*, Simultaneous Triplet Exciton-Phonon and Exciton-Photon Photoluminescence in the Individual Weak Confinement $CsPbBr_3$ Micro/Nanowires, *J. Phys. Chem. C*, 2019, **123**, 25349–25358.
43 Y. Zhang, S. Li, W. Yang, M. K. Joshi and X. Fang, Millimeter-Sized Single-Crystal $CsPbrB_3$/CuI Heterojunction for High-Performance Self-Powered Photodetector, *J. Phys. Chem. Lett.*, 2019, **10**, 2400–2407.
44 M. I. Saidaminov, *et al.*, Inorganic Lead Halide Perovskite Single Crystals: Phase-Selective Low-Temperature Growth, Carrier Transport Properties, and Self-Powered Photodetection, *Adv. Opt. Mater.*, 2017, **5**, 1600704.
45 Y. Yuan, *et al.*, Exciton recombination mechanisms in solution grown single crystalline $CsPbBr_3$ perovskite, *J. Lumin.*, 2020, **226**, 117471.
46 J. Di, *et al.*, Reveal the Humidity Effect on the Phase Pure $CsPbBr_3$ Single Crystals Formation at Room Temperature and Its Application for Ultrahigh Sensitive X-Ray Detector, *Adv. Sci.*, 2022, **9**, 2103482.
47 J. Ding, *et al.*, High Detectivity and Rapid Response in Perovskite $CsPbBr_3$ Single-Crystal Photodetector, *J. Phys. Chem. C*, 2017, **121**, 4917–4923.
48 Z. Liu, *et al.*, Defects of perovskite semiconductor $CsPbBr_3$ investigated via photoluminescence and thermally stimulated current spectroscopies, *J. Appl. Phys.*, 2023, **134**, 245101.
49 N. Falsini, *et al.*, Analysis of the Urbach tail in cesium lead halide perovskites, *J. Appl. Phys.*, 2022, **131**, 10902.
50 L. Su, Growth of a Sub-Centimeter-Sized $CsPbBr_3$ Bulk Single Crystal Using an Anti-Solvent Precipitation Method, *Symmetry*, 2024, **16**, 332.
51 J. H. Heo, H. J. Han, D. Kim, T. K. Ahn and S. H. Im, Hysteresis-less inverted $CH_3NH_3PbI_3$ planar perovskite hybrid solar cells with 18.1% power conversion efficiency, *Energy Environ. Sci.*, 2015, **8**, 1602–1608.
52 P. Zhao, *et al.*, Improved carriers injection capacity in perovskite solar cells by introducing A-site interstitial defects, *J. Mater. Chem. A*, 2017, **5**, 7905–7911.
53 A. Bouddouch, *et al.*, Photodegradation under UV Light Irradiation of Various Types and Systems of Organic Pollutants in the Presence of a Performant $BiPO_4$ Photocatalyst, *Catalysts*, 2022, **12**, 691.
54 T. Chen, J. Xie and P. Gao, Ultraviolet Photocatalytic Degradation of Perovskite Solar Cells: Progress, Challenges, and Strategies, *Adv. Energy Sustainability Res.*, 2022, **3**, 2100218.
55 G. Abdelmageed, *et al.*, Mechanisms for light induced degradation in MAPbI3 perovskite thin films and solar cells, *Appl. Phys. Lett.*, 2016, **109**, 233905.
56 J. Song, *et al.*, Ultralarge All-Inorganic Perovskite Bulk Single Crystal for High-Performance Visible–Infrared Dual-Modal Photodetectors, *Adv. Opt. Mater.*, 2017, **5**, 1–8.
57 P. Zhang, *et al.*, Anisotropic Optoelectronic Properties of Melt-Grown Bulk $CsPbBr_3$ Single Crystal, *J. Phys. Chem. Lett.*, 2018, **9**, 5040–5046.
58 X. Miao, *et al.*, Air-stable $CsPb1\text{-}xBixBr_3$ $(0 \leq x \ll 1)$ perovskite crystals: Optoelectronic and photostriction properties, *J. Mater. Chem. C*, 2017, **5**, 4931–4939.
59 H. Zhang, *et al.*, Centimeter-sized inorganic lead halide perovskite $CsPbBr_3$ crystals grown by an improved solution method, *Cryst. Growth Des.*, 2017, **17**, 6426–6431.